Structure of solvent-free grafted nanoparticles: Molecular dynamics and density-functional theory

Alexandros Chremos, Athanassios Z. Panagiotopoulos, Hsiu-Yu Yu, and Donald L. Koch

Citation: J. Chem. Phys. **135**, 114901 (2011); doi: 10.1063/1.3638179
View online: http://dx.doi.org/10.1063/1.3638179
View Table of Contents: http://jcp.aip.org/resource/1/JCPSA6/v135/i11
Published by the AIP Publishing LLC.

Structure of solvent-free grafted nanoparticles: Molecular dynamics and density-functional theory

Alexandros Chremos,[1] Athanassios Z. Panagiotopoulos,[1,a)] Hsiu-Yu Yu,[2] and Donald L. Koch[2]
[1]*Department of Chemical and Biological Engineering, Princeton University, Princeton, New Jersey 08544, USA*
[2]*School of Chemical and Biomolecular Engineering, Cornell University, Ithaca, New York 14853, USA*

(Received 20 June 2011; accepted 23 August 2011; published online 19 September 2011)

The structure of solvent-free oligomer-grafted nanoparticles has been investigated using molecular dynamics simulations and density-functional theory. At low temperatures and moderate to high oligomer lengths, the qualitative features of the core particle pair probability, structure factor, and the oligomer brush configuration obtained from the simulations can be explained by a density-functional theory that incorporates the configurational entropy of the space-filling oligomers. In particular, the structure factor at small wave numbers attains a value much smaller than the corresponding hard-sphere suspension, the first peak of the pair distribution function is enhanced due to entropic attractions among the particles, and the oligomer brush expands with decreasing particle volume fraction to fill the interstitial space. At higher temperatures, the simulations reveal effects that differ from the theory and are likely caused by steric repulsions of the expanded corona chains. © *2011 American Institute of Physics*. [doi:10.1063/1.3638179]

I. INTRODUCTION

Our understanding of statistical mechanics of simple liquids has seen a remarkable growth over the last decades,[1] and a considerable shift of focus towards understanding systems with higher complexity is currently taking place. An important line of research in soft matter is the study of nanoparticle suspensions.[2,3] There is already a significant body of literature describing their structural and transport properties,[4–9] and offering new ways for controlling their self-assembly.[10–12] Of particular interest for the present study are nanoparticle organic hybrid materials (NOHMs),[13–18] novel hybrid systems consisting of a hard (inorganic) core and a soft (organic) oligomer corona. Experiments have showed that by varying the molecular weight and grafting density of the arms and core particle size, systems can be designed with properties that span glasses, stiff waxes and gels (at high volume fractions), to simple liquids (at low volume fractions). The oligomer chains grafted to the nanoparticles not only prevent nanoparticle aggregation due to van der Waals attractions or depletion interactions, but also provide sufficient fluidity for the system to relax to a disordered equilibrium state even in the absence of an added solvent.

An oligomer grafted nanoparticle may begin to resemble a star polymer when the size of the core is much smaller than the radius of gyration of the oligomers; such an equivalence has been demonstrated for isolated particles.[19] The Daoud-Cotton model[20] provides a scaling theory for the properties of polymer brushes on curved surfaces[21–23] and in star polymer solutions.[21,24,25] Star polymer solutions interacting through pairwise steric-repulsive potentials have been shown to exhibit increased structure with increasing temperature[26,27] as a result of the expansion of the polymer chains with temperature.

Oligomer-grafted nanoparticles have been considered in previous theoretical studies in a phantom solvent to determine the effects of a single[28] and multiple grafted chains[29] on their structure. Particular emphasis has been placed recently in computational studies on self-assembly of grafted nanoparticles into shapes such as disks,[11] cubes,[30] rods,[31,32] and spheres.[33,34]

While theoretical studies of sterically stabilized particles have usually considered high molecular weight grafted polymers in the presence of a solvent, a recent study by Yu and Koch[35] has addressed the equilibrium structure of solvent-free oligomer-grafted nanoparticles using a coarse-grained density-functional theory. In Ref. 35, the tethered oligomers were treated as an incompressible fluid. Lagrange undetermined multipliers were used to enforce the constraint that the monomer number density remains constant within the fluid volume. Since all the surrounding nanoparticles contribute to this number density, the minimization of the oligomer free energy subject to this constraint leads to non-pairwise-additive potentials. Analytical results could be obtained nonetheless using a "weak field" approximation valid in the limit where the radius of gyration of the oligomers is large compared with the core radius, so that the contribution of each nanoparticle to the local monomer concentration is small. The incompressibility assumption is expected to hold when the attractive energy among the monomers is strong relative to the thermal energy.

In this paper, we focus on the effect of NOHMs architecture, including oligomer molecular weight and core radius, on the equilibrium structure of NOHMs, using coarse-grained molecular dynamics simulations (MD) and density-functional

a)Author to whom correspondence should be addressed. Electronic mail: azp@princeton.edu.

theory. In the MD simulations, each tethered oligomer is composed of 5 to 15 monomer beads connected with stiff springs which approximate freely jointed chains, with a cut-and-shifted Lennard-Jones (LJ) potential between their beads. We examine the structure factor and pair probability of the cores, the core-oligomer-bead correlation, and the structure of the oligomer brush. Computations at modest temperatures are used to explore the behavior of solvent-free NOHMs systems, whereas higher temperature simulations yield void spaces between the oligomers which may be interpreted in terms of the effects of an implicit solvent.

To obtain a density-functional theory appropriate for comparison with the molecular dynamics simulations, the incompressibility constraint invoked in Ref. 35 must be relaxed. In the modified theory, the free energy of the fluid of tethered oligomers includes a spring energy modeling the configurational free energy of the chains and the free energy density of a liquid of Lennard-Jones monomers. The local monomer number density results from the contributions of oligomers from all the neighboring particles. We will see that this formulation leads to results that agree with the incompressible NOHMs theory of Ref. 35 when the temperature is small such that $k_B T \leq \varepsilon$, where ε is the potential well depth of the LJ pair potential. The theory captures the qualitative changes in the pair probability, structure factor, and oligomer brush height observed in the MD with increasing temperature.

The paper is organized as follows. Section II contains details of the coarse-grained MD model, and the simulation methods. Section III describes the theoretical methodology. Results for the structure of oligomer grafted nanoparticles are presented in Sec. IV. Section V summarizes the conclusions.

II. SIMULATION METHODS

The system consists of N oligomer-grafted nanoparticles. Each nanoparticle is represented as a spherical core with f attached chains. Each chain is composed of N_m beads (or monomers). The core and monomers have radii a_c and a_b, respectively. We set the diameter of the monomers $\sigma = 2a_b$ as the unit of length; the core radius is $a_c = 2.5\sigma$. The oligomer grafting density is fixed as $\rho_s = f/(4\pi a_c^2) = 0.32\sigma^{-2}$ unless stated otherwise. Interactions between monomers are described by the cut-and-shifted Lennard-Jones potential with ε and σ as the energy and range parameters, and the cutoff distance $r_c = 2.5\sigma$,

$$V(r) = \begin{cases} 4\varepsilon\left[\left(\frac{\sigma}{r}\right)^{12} - \left(\frac{\sigma}{r}\right)^{6} - \left(\frac{\sigma}{r_c}\right)^{12} + \left(\frac{\sigma}{r_c}\right)^{6}\right] & r \leq r_c \\ 0 & r > r_c \end{cases}. \quad (1)$$

The initial bead of each chain is rigidly attached to the core surface; other monomers along a chain are connected with their neighbors via a stiff harmonic spring,

$$V_H(r) = k(r - l_0)^2, \quad (2)$$

where $l_0 = \sigma$ is the equilibrium length of the spring, and $k = 10\,000\varepsilon/\sigma^2$ is the spring constant. The core–core and core–monomer interactions are modelled as purely repulsive Weeks-Chandler-Andersen (WCA) potentials[36] with modification taking into account the difference in the particle sizes,[37]

$$V_{WCA}(r) = \begin{cases} 4\varepsilon\left[\left(\frac{\sigma}{r-\Delta_{ij}}\right)^{12} - \left(\frac{\sigma}{r-\Delta_{ij}}\right)^{6} + 0.25\right] & r \leq r_{min} \\ 0 & r > r_{min} \end{cases}, \quad (3)$$

where $r_{min} = 2^{1/6}(a_c + a_c)$ and $\Delta_{cc} = 2(a_c - a_b)$ for core–core interaction, and $r_{min} = 2^{1/6}(a_c + a_b)$ and $\Delta_{cb} = (a_c - a_b)$ for core–monomer interaction. The energy and interaction range parameters are chosen to be the same for these interactions such that $\varepsilon_{cc} = \varepsilon_{cb} = \varepsilon$ and $\sigma_{cc} = \sigma_{cb} = \sigma$. The choice of a purely repulsive interaction was based on the fact that typical inorganic nanoparticles and organic polymers have strongly unfavorable mutual interactions.

Simulations were performed in a cubic box of length L; periodic boundary conditions and the minimum-image convention were applied in all three directions. The simulations were performed by the large-scale atomic/molecular massively parallel simulator (LAMMPS) package[38] which takes advantage of a neighbor-list construction and communication algorithm, speeding up simulations when the ratio of sizes of the particles becomes large.[39] Figure 1(a) shows a typical configuration of a nanoparticle and Fig. 1(b) shows a solvent-free oligomer-grafted nanoparticle system with chain

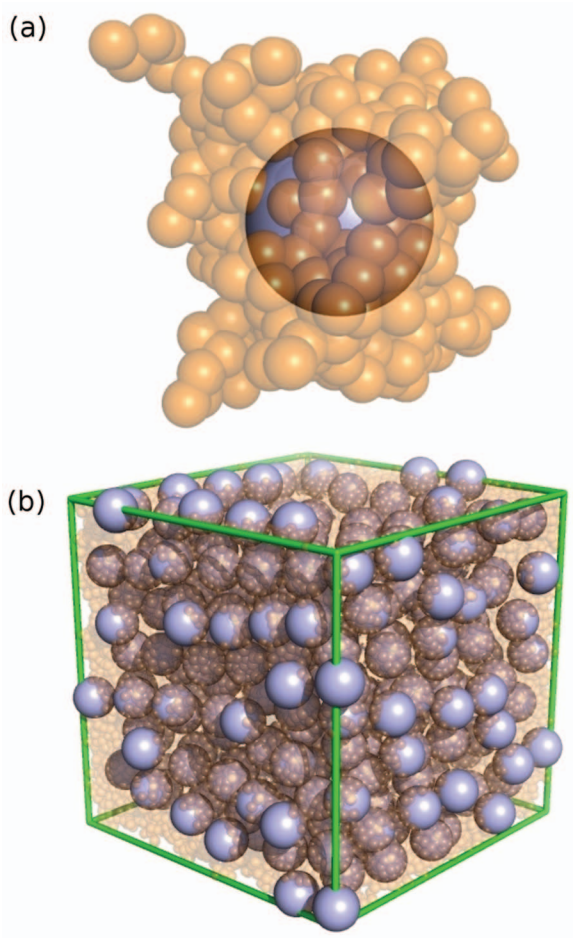

FIG. 1. (a) A nanoparticle with $N_m = 10$; (b) a system of 350 nanoparticles with $N_m = 5$ at volume fraction $\phi_c = 0.181$, and $T^* = 2.5$. The oligomer beads are transparent for visualization purposes in (a) and (b).

length $N_m = 5$. The mass of a particle scales linearly with volume, so that $m_b = m$ and $m_c = ma_c^3/a_b^3$ for the mass of the oligomer bead and core, respectively.

Simulations were performed in the NVE ensemble after equilibration in the NVT ensemble at the desired temperature. The equations of motion were integrated by the velocity-Verlet algorithm. Time averaging was conducted for $O(10^7)$ time steps after equilibration. The time step was set to $\delta t = 0.004\tau$, where $\tau = \sigma(\frac{m}{\varepsilon})^{1/2}$ is the unit of time. The reduced simulation units for the thermodynamic variables are: $T^* = k_B T/\varepsilon$ and $P^* = P\sigma^3/\varepsilon$. All simulations were performed at atmospheric pressure, which closely corresponds in reduced units to $P^* = 0$. This is achieved in the following way: for a given density, the temperature was chosen so that in the NVE ensemble the average reduced pressure was close to zero. The concentration of the cores can be described using the volume fraction, $\phi_c = N\frac{4\pi}{3}a_c^3/L^3$ and number density $\rho_c = N/L^3$, while the number density and volume fraction of the beads in the interstitial space between the cores are $\rho_b = NfN_m/(L^3 - N\frac{4\pi}{3}a_c^3)$ and $\phi_b = \frac{4\pi}{3}a_b^3 NfN_m/(L^3 - N\frac{4\pi}{3}a_c^3)$.

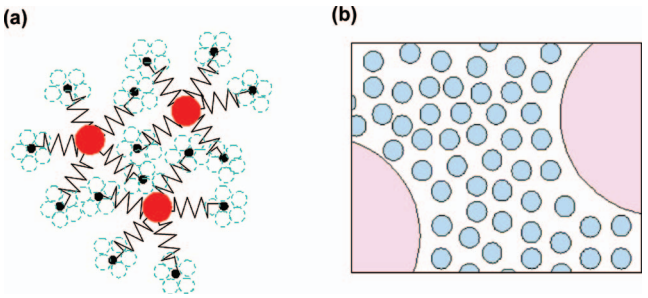

FIG. 2. (a) Schematic of the coarse-grained particle-scale model considered in this work. The big central spheres are the hard cores and the smaller dashed hollow beads represent the monomers. Each group of N_m monomers composes an oligomeric chain with the group's center of mass (smallest solid bead) being connected to the core with a linear spring. In this model the number of oligomers per particle and the number of monomers per chain are adjustable parameters f and N_m, and for clarity we only illustrate a few oligomers and monomers here. (b) A cartoon illustrating a homogeneous LJ monomers with a local volume fraction within the interparticle space. The size of the monomers is smaller than the cores and the springs are not shown for simplicity. In evaluating the local free energy density due to LJ interactions the connectivity of the beads is neglect; however, the spring energy in the overall expression for the free energy models the entropic penalty due to the beads' connection to the core.

III. THEORY

In the finite-core NOHMs model of Ref. 35, a pure NOHMs system was considered, consisting of hard cores and bead-spring oligomers attached to the centers of the cores with only one bead per chain at the free end of each spring. The monomer beads were treated as an incompressible fluid filling the interparticle space. In the MD simulations, the tethered-oligomer fluid is not strictly incompressible. However, the Lennard-Jones attractions among the monomers resist variations in the monomer number density. To capture this effect, we introduce the coarse-grained model shown in Fig. 2(a). In place of the incompressibility constraint we will incorporate a contribution to the free energy of the oligomers associated with the LJ interactions among a locally homogeneous fluid of monomers coming from all the adjacent cores. In the theory these LJ interactions correspond to the pair potential in Eq. (1) with no cutoff. To accurately mimic the LJ interactions in the MD we use the same number of beads per oligomer N_m as are used in the MD simulations. However, to simplify the theory, we consider these beads to form a cluster localized at the end of the oligomer. We only consider the translational free energy of each monomer group's center of mass and the oligomer configuration is described by linear springs with a rest length of zero. Whereas the stiff springs in the MD simulations connecting the neighboring monomers only differ from hard rods for computational convenience, the soft spring in the theory models the effect of the chain's configurational entropy. We parameterize the stiffness of the oligomer springs with the radius of gyration R_g of an ideal, unattached, linear chain such that the spring energy is defined by $F_{spring} = \frac{1}{4}\frac{k_B T}{R_g^2}r_f^2$ with r_f being the distance between the spring free end and the core center. The normalization of the configurational probability of each oligomer is

$$\int_V G(\mathbf{r}_f)d\mathbf{r}_f = 1, \tag{4}$$

and the mean-square distance of the spring free end from the core center in the absence of chain–chain interactions is

$$\langle r_f^2 \rangle = \int_V r_f^2 G(\mathbf{r}_f)d\mathbf{r}_f = 6R_g^2 \tag{5}$$

with V being the suspension volume. For simplicity, we relate the value of R_g in the theory to N_m and σ from the MD simulations using a model for unattached freely jointed chains (FJC) and obtain $\frac{R_g}{\sigma} = [\frac{1}{6}(\frac{N_m+2}{N_m+1})N_m]^{\frac{1}{2}}$.[40]

The theory exploits a weak oligomeric-field approximation valid when $R_g \gg a_c$, so that the monomers that fill any region of space come from many different cores. In this limit, we can use different approximations over two different length scales. For separations of order a_c hard-core interactions dominate, while the oligomeric interactions dominate at separations of order R_g. In the latter region, we can neglect the detailed packing configuration of the particles and assume that the particles simply fill a fraction ϕ_c of the space. The condition $\rho_c R_g^3 \gg 1$ also allows us to close the equations governing the oligomer concentration and the core radial distribution function by neglecting correlations smaller than $O(1/\rho_c R_g^3)$ or $O(a_c^3/R_g^3)$ as justified in Ref. 35.

We assume that the oligomers can relax quickly compared with the cores. Therefore we can first formulate the fluid phase free energy at equilibrium for a given particle configuration. The fluid phase free energy contains the oligomer-configurational entropy, spring energy, and monomer–monomer interactions. Assuming that the monomer radius is much smaller than the core radius, we can identify a mesoscopic volume in the interstitial space containing a large number of monomers and consider this volume to have the free energy density of a homogeneous LJ fluid with the local monomer concentration. Betancourt-Cárdenas *et al.* have proposed an equation of state for the LJ fluid based on a second order perturbation scheme for the excess free energy of the system at the same temperature and density as

the ideal gas.[41] They then fit the free energy to a power series in the bulk volume fraction of the LJ fluid defined by the temperature-dependent effective hard-core diameter. We have used their results for the free energy of the LJ fluid including the first order perturbation. We neglect the second order contributions, which are shown to be small in their work. We neglect the temperature dependence of the effective hard core diameter, approximating it as σ. Therefore the excess Helmholtz free energy per monomer accounting for the monomer–monomer interactions is

$$\Phi_{\mathrm{LJ}}(\phi_{\mathrm{b}}^{\mathrm{t}}) = \Phi_{\mathrm{LJ}}^{\mathrm{HS}}(\phi_{\mathrm{b}}^{\mathrm{t}}) + \frac{\varepsilon}{k_{\mathrm{B}}T}\Phi'_{\mathrm{LJ}}(\phi_{\mathrm{b}}^{\mathrm{t}}), \tag{6}$$

where $\Phi_{\mathrm{LJ}}^{\mathrm{HS}}$ is the free energy of the reference hard sphere monomer fluid, Φ'_{LJ} is the first order perturbation to the free energy due to the LJ interaction. This free energy per monomer is a direct function of the local monomer volume fraction in the fluid phase defined by $\phi_{\mathrm{b}}^{\mathrm{t}}(\mathbf{r}_{\mathrm{f}}) = \frac{\pi}{6}\frac{\sigma^3 N_{\mathrm{m}}}{1-\phi_{\mathrm{c}}}\sum_{i=1}^{N} C_i(\mathbf{r}_{\mathrm{f}}, \mathbf{r}_i)$ at $\mathbf{r}_{\mathrm{f}}$. Here $1-\phi_{\mathrm{c}}$ in the denominator takes into account that the cores occupy a fraction ϕ_{c} of the volume and $C_i(\mathbf{r}_{\mathrm{f}}, \mathbf{r}_i)$ is the concentration at a position $\mathbf{r}_{\mathrm{f}}$ of oligomers that are attached to particle i at $\mathbf{r}_i$. For a system of N particles, each of which has f tethered oligomers composed of N_{m} monomers, the fluid phase free energy is written as

$$\frac{F_{\mathrm{f}}}{k_{\mathrm{B}}T} = \sum_{i=1}^{N}\int_V C_i(\mathbf{r}_{\mathrm{f}}, \mathbf{r}_i)\left[\ln C_i(\mathbf{r}_{\mathrm{f}}, \mathbf{r}_i)\Lambda_{\mathrm{b}}^3 - 1\right] + \frac{1}{4R_{\mathrm{g}}^2}(\mathbf{r}_{\mathrm{f}} - \mathbf{r}_i)^2 C_i(\mathbf{r}_{\mathrm{f}}, \mathbf{r}_i) + \frac{\Phi_{\mathrm{LJ}}}{k_{\mathrm{B}}T}N_{\mathrm{m}}C_i(\mathbf{r}_{\mathrm{f}}, \mathbf{r}_i)\mathrm{d}\mathbf{r}_{\mathrm{f}}, \tag{7}$$

where Λ_{b} is the thermal de Broglie wavelength of the beads. Since each oligomer consists of N_{m} beads, $N_{\mathrm{m}}C_i(\mathbf{r}_{\mathrm{f}}, \mathbf{r}_i)$ is the concentration of monomer beads from particle i. In this expression, the first term represents the ideal gas Helmholtz free energy of each N_{m}-monomer group's center of mass, the second term accounts for the spring energy, and the last term is introduced for the LJ interactions among the monomers and Φ_{LJ} is also a function of the oligomer concentration field. In a liquid, the attractive interactions lead to very little variation of the total volume fraction and so we may expect this last term to approximate an incompressibility constraint especially at small T^*.

The equilibrium concentration field of the oligomers can be determined by minimizing the fluid phase free energy with respect to variations in C_i subject to the constraint that the probability of finding the oligomers attached to a given particle is normalized,

$$\int_V C_i(\mathbf{r}_{\mathrm{f}}, \mathbf{r}_i)\mathrm{d}\mathbf{r}_{\mathrm{f}} = f. \tag{8}$$

This constraint can be applied by defining the Lagrange function,

$$L_{\mathrm{f}}[C_i(\mathbf{r}_{\mathrm{f}}, \mathbf{r}_i)] = \frac{F_{\mathrm{f}}}{k_{\mathrm{B}}T} - \sum_{i=1}^{N}\lambda_i\left[\int_V C_i(\mathbf{r}_{\mathrm{f}}, \mathbf{r}_i)\mathrm{d}\mathbf{r}_{\mathrm{f}} - f\right], \tag{9}$$

where the Lagrange multipliers λ_i enforcing the normalization make up a discrete set with one multiplier for each particle. For a given particle configuration, the minimization $\delta L_{\mathrm{f}}/\delta C_i(\mathbf{r}_{\mathrm{f}}, \mathbf{r}_i)$ yields

$$C_i(\mathbf{r}_{\mathrm{f}}, \mathbf{r}_i) = \frac{1}{\Lambda_{\mathrm{b}}^3}\exp\left\{\lambda_i - \frac{1}{4R_{\mathrm{g}}^2}(\mathbf{r}_{\mathrm{f}} - \mathbf{r}_i)^2 - \frac{N_{\mathrm{m}}}{k_{\mathrm{B}}T}\left[\Phi_{\mathrm{LJ}}\Big|_{\mathbf{r}_{\mathrm{f}}} + \phi_{\mathrm{b}}^{\mathrm{t}}(\mathbf{r}_{\mathrm{f}})\frac{\partial\Phi_{\mathrm{LJ}}}{\partial\phi_{\mathrm{b}}^{\mathrm{t}}}\Big|_{\mathbf{r}_{\mathrm{f}}}\right]\right\}. \tag{10}$$

When $R_{\mathrm{g}}^3 \gg a_{\mathrm{c}}^3$, many particles' oligomers contribute to the local fluid density at $\mathbf{r}_{\mathrm{f}}$ and each particle's oligomers only cause a small $O(a_{\mathrm{c}}^3/R_{\mathrm{g}}^3)$ disturbance to the fluid density. Therefore we can linearize the monomer volume fraction and the LJ free energy per monomer by writing $\phi_{\mathrm{b}}^{\mathrm{t}}(\mathbf{r}_{\mathrm{f}}) = \phi_{\mathrm{b}} + \phi'_{\mathrm{b}}(\mathbf{r}_{\mathrm{f}})$, $\Phi_{\mathrm{LJ}}|_{\mathbf{r}_{\mathrm{f}}} = \Phi_{\mathrm{LJ}}^0 + \frac{\partial\Phi_{\mathrm{LJ}}^0}{\partial\phi_{\mathrm{b}}}\phi'_{\mathrm{b}}(\mathbf{r}_{\mathrm{f}})$, and $\frac{\partial\Phi_{\mathrm{LJ}}}{\partial\phi_{\mathrm{b}}^{\mathrm{t}}}|_{\mathbf{r}_{\mathrm{f}}} = \frac{\partial\Phi_{\mathrm{LJ}}^0}{\partial\phi_{\mathrm{b}}} + \frac{\partial^2\Phi_{\mathrm{LJ}}^0}{\partial\phi_{\mathrm{b}}^2}\phi'_{\mathrm{b}}(\mathbf{r}_{\mathrm{f}})$ with Φ_{LJ}^0 being evaluated using the average bead volume fraction ϕ_{b}. The deviation of the bead volume fraction from its average $\phi'_{\mathrm{b}}(\mathbf{r}_{\mathrm{f}}) = O(a_{\mathrm{c}}^3/R_{\mathrm{g}}^3)$. Keeping terms up to linear order in $\phi'_{\mathrm{b}}(\mathbf{r}_{\mathrm{f}})$ for the LJ interactions and making use of Eq. (6), we obtain

$$C_i(\mathbf{r}_{\mathrm{f}}, \mathbf{r}_i) = f\Lambda_i B(\mathbf{r}_{\mathrm{f}})G(\mathbf{r}_{\mathrm{f}} - \mathbf{r}_i), \tag{11}$$

where $G(\mathbf{r}_{\mathrm{f}} - \mathbf{r}_i) = (4\pi R_{\mathrm{g}}^2)^{-\frac{3}{2}}e^{-\frac{(\mathbf{r}_{\mathrm{f}}-\mathbf{r}_i)^2}{4R_{\mathrm{g}}^2}}$ is the probability of finding a monomer bead in the absence of particle interactions, $B(\mathbf{r}_{\mathrm{f}}) = e^{-N_{\mathrm{m}}\phi'_{\mathrm{b}}(\mathbf{r}_{\mathrm{f}})f_{\mathrm{LJ}}}$ with $f_{\mathrm{LJ}} = \frac{1}{k_{\mathrm{B}}T}[2\frac{\partial\Phi_{\mathrm{LJ}}^0}{\partial\phi_{\mathrm{b}}} + \phi_{\mathrm{b}}\frac{\partial^2\Phi_{\mathrm{LJ}}^0}{\partial\phi_{\mathrm{b}}^2}]$ accounts for the change in the monomer concentration due to particle interactions, and Λ_i is a normalization constant. When $R_{\mathrm{g}}^3 \gg a_{\mathrm{c}}^3$, we can write $B(\mathbf{r}_{\mathrm{f}}) = 1 + B'(\mathbf{r}_{\mathrm{f}})$ and $\Lambda_i = 1 + \Lambda'_i$ where the perturbations $B'(\mathbf{r}_{\mathrm{f}})$ and Λ'_i are $O(a_{\mathrm{c}}^3/R_{\mathrm{g}}^3)$. In particular, $B'(\mathbf{r}_{\mathrm{f}}) = -N_{\mathrm{m}}\phi'_{\mathrm{b}}(\mathbf{r}_{\mathrm{f}})f_{\mathrm{LJ}}$.

The total concentration of oligomers obtained by summing oligomers attached to all cores is $C(\mathbf{r}_{\mathrm{f}}) = \sum_{i=1}^{N} C_i(\mathbf{r}_{\mathrm{f}}, \mathbf{r}_i) = \rho_{\mathrm{c}}f[1 + \frac{\phi'_{\mathrm{b}}(\mathbf{r}_{\mathrm{f}})}{\phi_{\mathrm{b}}}]$. Following the procedure used in Ref. 35, we derive an equation for the conditional average concentration $\langle C_1\rangle_1(\mathbf{r}_{\mathrm{f}}|\mathbf{r}_1)$ with one core particle fixed at $\mathbf{r}_1$ as

$$\langle C\rangle_1(\mathbf{r}_{\mathrm{f}}|\mathbf{r}_1) = \langle C_1\rangle_1(\mathbf{r}_{\mathrm{f}}|\mathbf{r}_1) + \rho_{\mathrm{c}}\int_V g_{\mathrm{cc}}(\mathbf{r}_2 - \mathbf{r}_1)\langle C_2\rangle_2(\mathbf{r}_{\mathrm{f}}|\mathbf{r}_1, \mathbf{r}_2)\mathrm{d}\mathbf{r}_2 = \rho_{\mathrm{c}}f\left[1 + \frac{\langle\phi'_{\mathrm{b}}\rangle_1(\mathbf{r}_{\mathrm{f}}|\mathbf{r}_1)}{\phi_{\mathrm{b}}}\right], \tag{12}$$

where $\rho_{\mathrm{c}} = \frac{N}{V} \approx \frac{N-1}{V}$, $\langle C_1\rangle_1(\mathbf{r}_{\mathrm{f}}|\mathbf{r}_1)$ is the conditional average of the concentration field of oligomers attached to particle 1 given that particle 1 is fixed at $\mathbf{r}_1$, $\langle C_2\rangle_2(\mathbf{r}_{\mathrm{f}}|\mathbf{r}_1, \mathbf{r}_2)$ is the conditional average of the concentration field of oligomers attached to particle 2 given that particles 1 and 2 are fixed at $\mathbf{r}_1$ and $\mathbf{r}_2$, and $g_{\mathrm{cc}}(\mathbf{r}_2 - \mathbf{r}_1)$ is the radial distribution function. Under the weak-field approximation,

$$\langle C_1\rangle_1(\mathbf{r}_{\mathrm{f}}|\mathbf{r}_1) \approx f[1 + \langle\Lambda'_1\rangle_1(\mathbf{r}_1|\mathbf{r}_1) + \langle B'\rangle_1(\mathbf{r}_{\mathrm{f}}|\mathbf{r}_1)]G(\mathbf{r}_{\mathrm{f}} - \mathbf{r}_1), \tag{13}$$

$$\langle C_2\rangle_2(\mathbf{r}_f|\mathbf{r}_1,\mathbf{r}_2) \approx f[1+\langle\Lambda_2'\rangle_1(\mathbf{r}_2|\mathbf{r}_2) + \langle\Lambda_2''\rangle_2(\mathbf{r}_2|\mathbf{r}_1,\mathbf{r}_2) + \langle B'\rangle_1(\mathbf{r}_f|\mathbf{r}_1) + \langle B'\rangle_1(\mathbf{r}_f|\mathbf{r}_2)]G(\mathbf{r}_f-\mathbf{r}_2), \quad (14)$$

$$g_{cc}(\mathbf{r}_2-\mathbf{r}_1) = 1 + h_{HS}(\mathbf{r}_2-\mathbf{r}_1) + h_f(\mathbf{r}_2-\mathbf{r}_1), \quad (15)$$

where h_{HS} is the total correlation function of the reference hard sphere suspension without the oligomers and h_f is the perturbation to the hard sphere pair distribution function due to the oligomers. The conditional average field variables and h_f are of $O(a_c^3/R_g^3)$. Substituting Eqs. (13)–(15) into Eq. (12) and retaining terms of order one yields

$$G(\mathbf{r}_f-\mathbf{r}_1) + \rho_c\int_V [\langle\Lambda_2'\rangle_1(\mathbf{r}_2|\mathbf{r}_2) + \langle\Lambda_2''\rangle_2(\mathbf{r}_2|\mathbf{r}_1,\mathbf{r}_2) + \langle B'\rangle_1(\mathbf{r}_f|\mathbf{r}_1) + \langle B'\rangle_1(\mathbf{r}_f|\mathbf{r}_2) + h_{HS}(\mathbf{r}_2-\mathbf{r}_1) + h_f(\mathbf{r}_2-\mathbf{r}_1)]G(\mathbf{r}_f-\mathbf{r}_2)d\mathbf{r}_2 = \rho_c\frac{\langle\phi_b'\rangle_1(\mathbf{r}_f|\mathbf{r}_1)}{\phi_b}. \quad (16)$$

Application of the normalization conditions for $\langle C_1\rangle_1$ and $\langle C_2\rangle_2$ and Fourier transformation of Eq. (16) yield the field variables required to obtain the oligomer concentration field to $O(a_c^3/R_g^3)$,

$$\langle\hat{B}'\rangle_1(\mathbf{q}) = -N_m f_{LJ}\langle\hat{\phi}_b'\rangle_1(\mathbf{q}) = \frac{\hat{G}(\mathbf{q})\left[1+\rho_c\hat{h_{HS}}(\mathbf{q})+\rho_c\hat{h_f}(\mathbf{q})\right]}{\rho_c\left[\hat{G}(\mathbf{q})^2 - 1 - \frac{1}{N_m f_{LJ}\phi_b}\right]}, \quad (17)$$

$$\langle\hat{\Lambda}_2''\rangle_2(\mathbf{q}) = -\langle\hat{B}'\rangle_1(\mathbf{q})\hat{G}(\mathbf{q}), \quad (18)$$

$$\langle\Lambda_i'\rangle_1(\mathbf{r}_i|\mathbf{r}_i) = -\frac{1}{(2\pi)^3}\int_{V_q}\langle\hat{B}'\rangle_1(\mathbf{q})\hat{G}(-\mathbf{q})d\mathbf{q} \quad (19)$$

with V_q being an unbounded wave number space. As $\mathbf{q}\to 0$, $\hat{G}(\mathbf{0}) = 1$. The Fourier transform of $F(\mathbf{x})$ and the inverse transform of $\hat{F}(\mathbf{s})$ are defined by $\hat{F}(\mathbf{s}) = \int F(\mathbf{x})e^{-i\mathbf{s}\cdot\mathbf{x}}d\mathbf{x}$ and $F(\mathbf{x}) = \frac{1}{(2\pi)^3}\int\hat{F}(\mathbf{s})e^{i\mathbf{s}\cdot\mathbf{x}}d\mathbf{s}$.

We apply a density-functional approach similar to Ref. 35 to solve for the radial distribution function. The grand potential Ω of the entire system given that a *chosen* particle labeled 1 is at the origin can be expressed as a functional of the one-body density profile of other *non-chosen* particles labeled 2 around particle 1, $\rho_c^t(\mathbf{r}) = \rho_c g_{cc}(\mathbf{r})$, with $\mathbf{r}$ being $\mathbf{r}_2-\mathbf{r}_1$,

$$\Omega[\rho_c^t(\mathbf{r})] = F_{id}[\rho_c^t(\mathbf{r})] + F_{ex}^{HS}[\rho_c^t(\mathbf{r})] + F_{ex}^{fluid}[\rho_c^t(\mathbf{r})] + \int_V\rho_c^t(\mathbf{r})[V_1(\mathbf{r})-\mu]d\mathbf{r}, \quad (20)$$

where the ideal gas part of the free energy functional of the cores is

$$\frac{F_{id}[\rho_c^t(\mathbf{r})]}{k_BT} = \int_V\rho_c^t(\mathbf{r})\{\ln[\rho_c^t(\mathbf{r})\Lambda_p^3]-1\}d\mathbf{r} \quad (21)$$

with Λ_p being the thermal de Broglie wavelength of the particles, μ is the chemical potential of the particles, V_1 is the external potential due to the hard-sphere excluded volume of the fixed particle 1, F_{ex}^{HS} is the excess free energy contributed from the hard spheres, and F_{ex}^{fluid} is the excess free energy contributed from the fluid phase oligomers. For a given core configuration, the free energy of the oligomers is smeared out as a "mediated interparticle potential" between the cores. Therefore we obtain F_{ex}^{fluid} by conditionally averaging the fluid phase free energy shown in Eq. (7) over the configuration of $N-1$ particles given that particle 1 is fixed at the origin,

$$\frac{F_{ex}^{fluid}[\rho_c^t(\mathbf{r})]}{k_BT} = \left\langle\frac{F_f}{k_BT}\right\rangle_1 = \int_V\langle C_1\ln C_1\Lambda_b^3\rangle_1(\mathbf{r}_f|\mathbf{0}) + \left[\frac{\mathbf{r}_f^2}{4R_g^2}-1\right]\times\langle C_1\rangle_1(\mathbf{r}_f|\mathbf{0})d\mathbf{r}_f + \int_V\rho_c^t(\mathbf{r})\int_V\langle C_2\ln C_2\Lambda_b^3\rangle_2(\mathbf{r}_f|\mathbf{0},\mathbf{r}) + \left[\frac{(\mathbf{r}_f-\mathbf{r})^2}{4R_g^2}-1\right]\langle C_2\rangle_2(\mathbf{r}_f|\mathbf{0},\mathbf{r})d\mathbf{r}_f d\mathbf{r} + \frac{N_m}{k_BT}\int_V\langle C_1\Phi_{LJ}\rangle_1(\mathbf{r}_f|\mathbf{0})d\mathbf{r}_f + \frac{N_m}{k_BT}\int_V\rho_c^t(\mathbf{r})\times\int_V\langle C_2\Phi_{LJ}\rangle_2(\mathbf{r}_f|\mathbf{0},\mathbf{r})d\mathbf{r}_f d\mathbf{r}, \quad (22)$$

where $\mathbf{r}$ is the position of neighboring core particles labeled 2 and $\mathbf{r}_f$ is the position of beads.

At equilibrium, the minimization $\delta\Omega[\rho_c^t(\mathbf{r})]/\delta\rho_c^t(\mathbf{r}) = 0$ and application of equal chemical potential of the neighboring particles, $\mu = \mu_{bulk} = \mu|_{\mathbf{r}\to\infty}$, yield

$$\rho_c^t(\mathbf{r}) = \rho_c g_{cc}(\mathbf{r}) = \rho_c\exp\{c_{HS}^{(1)}(\mathbf{r}) - c_{HS,b}^{(1)} - V_1(\mathbf{r})/k_BT + c_f^{(1)}(\mathbf{r}) - c_{f,b}^{(1)}\}, \quad (23)$$

where the one-body direct correlation functions are defined by $c_{HS}^{(1)}(\mathbf{r}) = -\frac{\delta(F_{ex}^{HS}[\rho_c^t(\mathbf{r})]/k_BT)}{\delta\rho_c^t(\mathbf{r})}$, $c_{HS,b}^{(1)} = -\frac{\delta(F_{ex}^{HS}[\rho_c^t(\mathbf{r})]/k_BT)}{\delta\rho_c^t(\mathbf{r})}|_{\mathbf{r}\to\infty}$, $c_f^{(1)}(\mathbf{r}) = -\frac{\delta(F_{ex}^{fluid}[\rho_c^t(\mathbf{r})]/k_BT)}{\delta\rho_c^t(\mathbf{r})}$, and $c_{f,b}^{(1)} = -\frac{\delta(F_{ex}^{fluid}[\rho_c^t(\mathbf{r})]/k_BT)}{\delta\rho_c^t(\mathbf{r})}|_{\mathbf{r}\to\infty}$. As justified in Ref. 35, under the weak-field approximation and the separation of length scales, $R_g/a_c \gg 1$, we can obtain the core pair probability expressed in Eq. (15) with $1+h_{HS}(\mathbf{r}) = e^{[c_{HS}^{(1)}(\mathbf{r})-c_{HS,b}^{(1)}-V_1(\mathbf{r})/k_BT]}$ and $h_f(\mathbf{r}) \approx [c_f^{(1)}(\mathbf{r}) - c_{f,b}^{(1)}]$. Again, keeping dominant contributions from these variations of the free energy allows us to neglect the coupling between h_{HS} and h_f and we have $c_f^{(1)}(\mathbf{r}) \approx -\frac{\delta(F_{ex}^{fluid}[\rho_c^t(\mathbf{r})]/k_BT)}{\rho_c\delta h_f(\mathbf{r})}$ and $c_{HS}^{(1)}(\mathbf{r}) \approx -\frac{\delta(F_{ex}^{HS}[\rho_c^t(\mathbf{r})]/k_BT)}{\rho_c\delta h_{HS}(\mathbf{r})}$. Therefore we can directly evaluate h_{HS} by solving the Ornstein–Zernike equation with the Percus–Yevick approximation,[1,42] as done in Ref. 35. Substitution of the field variables Λ_i and $B(\mathbf{r}_f)$ into $F_{ex}^{fluid}[\rho_c^t(\mathbf{r})]/k_BT$ shown in Eq. (22), truncation of the higher order correlations between the particles, and functional differentiation $\frac{\delta(F_{ex}^{fluid}[\rho_c^t(\mathbf{r})]/k_BT)}{\rho_c\delta h_f(\mathbf{r})}$ finally yield to $O(a_c^3/R_g^3)$,

$$h_f(\mathbf{r}) \approx 2f\left(1-\frac{1}{f_{LJ}k_BT}\frac{\partial\Phi_{LJ}^0}{\partial\phi_b}\right)\int_V\langle\Lambda_2''\rangle_2(\mathbf{r}'|\mathbf{0},\mathbf{r})\frac{\delta\langle\Lambda_2''\rangle_2(\mathbf{r}'|\mathbf{0},\mathbf{r})}{\delta h_f(\mathbf{r})}d\mathbf{r}' - 2f\left(1-\frac{1}{f_{LJ}k_BT}\frac{\partial\Phi_{LJ}^0}{\partial\phi_b}\right)\int_V\langle B'\rangle_1(\mathbf{r}_f'|\mathbf{0})\frac{\delta\langle B'\rangle_1(\mathbf{r}_f'|\mathbf{0})}{\delta h_f(\mathbf{r})}d\mathbf{r}_f'. \quad (24)$$

This integral is convergent since the changes in the field variables due to the pair probability is important only within a distance $\sim R_g$ from the fixed particle 1. When particle 2 is deep in the bulk $\delta\langle\Lambda_2''\rangle_2(\mathbf{r}'|\mathbf{0},\mathbf{r})/\delta h_f(\mathbf{r})$ and $\delta\langle B'\rangle_1(\mathbf{r}_f'|\mathbf{0})/\delta h_f(\mathbf{r})$ are essentially zero. After making use of the convolution theorem and the expressions for $\langle\hat{B}'\rangle_1(\mathbf{q})$ and $\langle\hat{\Lambda}_2''\rangle_2(\mathbf{q})$, in Fourier space we obtain

$$\hat{h}_f(\mathbf{q}) = \frac{2f}{\rho_c}\left\{\frac{\left(\frac{1}{f_{LJ}k_BT}\frac{\partial\Phi_{LJ}^0}{\partial\phi_b}-1\right)\hat{G}(\mathbf{q})^2[1-\hat{G}(\mathbf{q})^2][1+\rho_c\hat{h}_{HS}(\mathbf{q})]}{\left[\hat{G}(\mathbf{q})^2-1-\frac{1}{N_m f_{LJ}\phi_b}\right]^2-2f\left(\frac{1}{f_{LJ}k_BT}\frac{\partial\Phi_{LJ}^0}{\partial\phi_b}-1\right)\hat{G}(\mathbf{q})^2[1-\hat{G}(\mathbf{q})^2]}\right\}. \quad (25)$$

The static structure factor of the cores is defined by $S(\mathbf{q}) = 1 + \rho_c\hat{h}_{HS}(\mathbf{q}) + \rho_c\hat{h}_f(\mathbf{q})$ and the core pair probability $g_{cc}(\mathbf{r})$ can be obtained by taking the inverse Fourier transform of $\hat{h}_f$ in Eq. (25) and adding the hard sphere pair probability. In statistical mechanics the value of $S(0)$ quantifies the compressibility of a single-component fluid.[1] We can see from Eq. (17) that for a finite LJ attraction well f_{LJ} is also finite and the monomer density fluctuations due to a fixed particle at very large length scales is determined by the compressibility of the system or the static structure factor when $\mathbf{q}\to\mathbf{0}$. In fact, Eq. (25) shows that for a finite f_{LJ}, $\hat{h}_f(\mathbf{0}) = 0$ and $S(\mathbf{0})$ retains the value of the reference hard sphere system at $\mathbf{q} = \mathbf{0}$. On the other hand, in the asymptotic limit as the attraction well is deep such that $f_{LJ}\to\infty$, we obtain $\frac{1}{N_m f_{LJ}\phi_b}\to 0$ and Eq. (25) can be reduced to Eq. (29) in Ref. 35 for incompressible single-component NOHMs systems.

Some results for the static structure factor at a fixed ϕ_c and different T^* calculated from the current LJ theory are compared with the results of the incompressible theory[35] and the reference hard sphere suspension in Fig. 3. We can see that at each temperature $S(q)$ shows hard-core correlations at large q and as we decrease q the deficit of particles around a fixed particle corresponding to the length scale of R_g occurs. This deficit is then followed by a plateau region at moderate to large length scales (roughly between $0.5 < q\cdot 2a_c < 2.5$ for the temperatures investigated here) characterizing suppressed density fluctuations. Eventually, as q approaches zero, $S(q)$ rises and yields $S(0)$ for the reference hard sphere system. The plateau region spans a larger range of q with decreasing T^*. For the incompressible case, the deficit of the particle continues as $q\to 0$ leading to $S(0) = 0$.

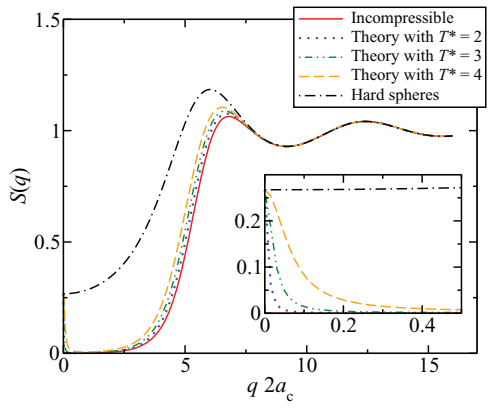

FIG. 3. Theoretical predictions for the static structure factor S as a function of the scaled wave number $q\cdot 2a_c$ for NOHMs with $\phi_c = 0.169$, $f = 25$, and $R_g/a_c = 0.540$ at different T^*. The monomer density as a function of T^* was taken to be equal to the MD simulation values: $\rho_b = 0.576$ for $T^* = 2$, $\rho_b = 0.395$ for $T^* = 3$, and $\rho_b = 0.228$ for $T^* = 4$. The solid line indicates the incompressible oligomeric fluid theory of Ref. 35 and the dashed-dotted line a hard sphere suspension. The inset shows the rise in $S(q)$ for the LJ theory at extremely small q.

IV. RESULTS AND DISCUSSION

The core volume fraction in solvent-free NOHMs can be altered by changing the oligomer grafting density, chain length, or temperature at zero pressure. In this study, we fix f but vary N_m and T^*. We have studied three different systems, with chain length N_m being equal to 5, 10, and 15. A wide range of temperatures ($T^* = 1.0$ up to 4.5) and volume fractions at zero pressure have been explored. Theoretical results are obtained based on the input parameters from the MD simulations: T^*, ρ_b, ϕ_c, f, and N_m. The values of R_g/a_c chosen in the theory are 0.394 for 5-mer chains, 0.540 for 10-mer chains, and 0.652 for 15-mer chains based on the FJC model. This indicates that the comparison of theory and MD simulation requires extending the theory beyond the weak field limit $R_g/a_c \gg 1$ for which it was derived.

When the thermal energy is sufficiently weak, the limit of high f_{LJ} can be achieved and the system is nearly incompressible. In Fig. 4, the core radial distribution function, $g_{cc}(r)$, and the static structure factor for a system with 25 10-mer chains per particle at $T^* = 1$ obtained from simulations and theory are plotted. The results obtained from the current LJ theory and from Yu and Koch's previous incompressible theory[35] are indistinguishable at the scale of the graph. Both theoretical and simulation results for $g_{cc}(r)$ show enhanced peaks and a smaller distance between the first and second peaks than the reference hard sphere suspension. Specifically, the maximum value of the first peak predicted by the theory is 2.16, which is comparable with the value 2.24 obtained from the simulations and larger than the value 1.57 for hard spheres. These observations are qualitatively different from Ref. 35 where R_g/a_c was greater than 1 and the oligomers generally produced a soft shell around the hard cores and reduced the contact value of $g_{cc}(r)$. Here we have fairly small R_g/a_c and the

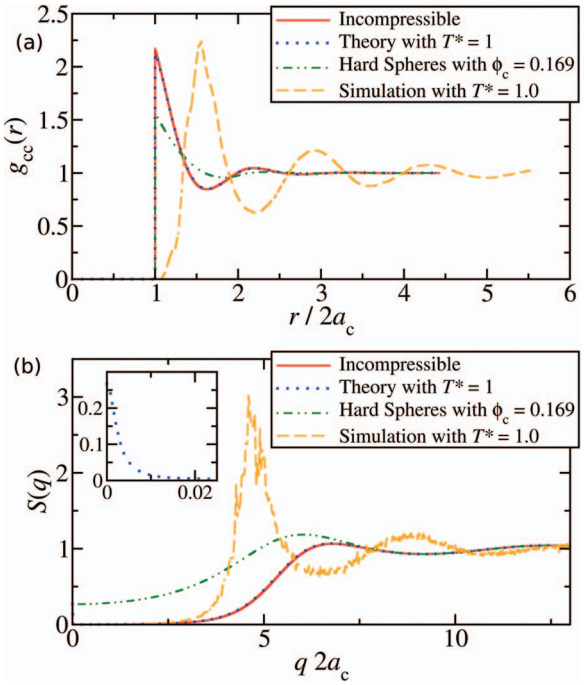

FIG. 4. (a) The radial distribution function g_{cc} as a function of the scaled interparticle distance $r/2a_c$ for the system with $f = 25$, $N_m = 10$, $\phi_c = 0.169$, and $\rho_b = 0.774$ at $T^* = 1$ predicted by the current LJ theory with $R_g/a_c = 0.540$ and the simulations. The results for the reference hard sphere suspension and for the incompressible system (Ref. 35) for the same f, ϕ_c, and R_g/a_c are also shown. (b) The corresponding comparison of the static structure factor S as a function of the scaled wave number $q \cdot 2a_c$. The lines are defined as in (a). The inset shows the rise in $S(q)$ for the LJ theory at extremely small q.

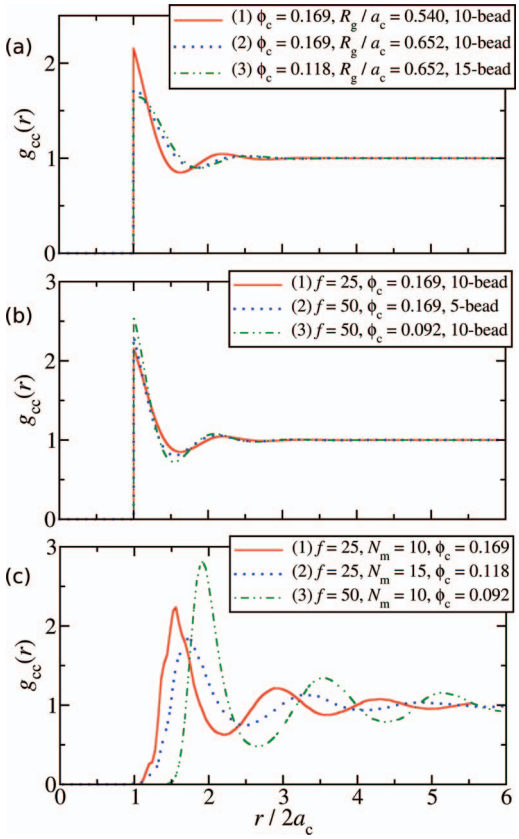

FIG. 5. (a) The radial distribution function g_{cc} as a function of the scaled interparticle distance $r/2a_c$ predicted by the LJ theory for different systems at $T^* = 1$ and $f = 25$: (1) the base system with $\rho_b = 0.774$, (2) the system with increased R_g/a_c but same ϕ_c and ρ_b as (1), and (3) the system with increased R_g/a_c and decreased ϕ_c; $\rho_b = 0.769$. (b) Similar to (a) but $T^* = 1$ and $R_g/a_c = 0.540$: (1) the same base system as (a), (2) the system with f doubled but same ϕ_c and ρ_b as (1), and (3) the system with doubled f and decreased ϕ_c; $\rho_b = 0.774$. (c) Simulation results: (1) base system with $T^* = 1$ and $\rho_b = 0.774$, (2) with longer chain length, $T^* = 1$, and $\rho_b = 0.769$, and (3) with higher grafting density, $T^* = 1.25$, and $\rho_b = 0.775$.

stiff space-filling oligomers yield a substantial attraction between the neighboring particles. The next nearest neighbors experience a similar attraction leading to a more structured core pair probability. While the theories predict the first peak at $r = 2a_c = 5\sigma$, the peaks are shifted to larger particle separations in the simulations. In the MD model, the first layer of monomers are rigidly grafted to the nanoparticle and this limits the ability of the cores to penetrate into separations between core-plus-grafted-monomer diameter 7σ and the core diameter 5σ. As a result, the simulations yield a gradual rise of $g_{cc}(r)$ over the range 5–7σ rather than the step change corresponding to hard sphere repulsion.

Figure 4 shows that the structure factor obtained by theory and simulation of NOHMs at $T^* = 1$ is greatly reduced compared to the hard sphere result when $q \cdot 2a_c < 2$. This indicates that a core excludes almost exactly one neighboring core from a neighborhood around its center. In the incompressible theory, $S(0) = 0$, whereas in the theory and simulations for LJ monomer interactions S reaches a plateau value around 0.01. At very small q, the theory predicts that $S(q)$ will rise and reach the hard sphere value at $q = 0$. This rise is not observed in the simulations. However, both theory and simulations indicate that density fluctuations are strongly damped at large length scales. Both theoretical and simulation $S(q)$ exhibit peaks corresponding to nearest and next nearest neighbor interactions for $q \cdot 2a_c \geq 3$. These peaks in the MD simulations are enhanced relative to the hard sphere peaks due to the enhancement of the core–core repulsion by the first layer of grafted monomers as discussed above.

After justifying the incompressible nature of the system at $T^* = 1$, it is of interest to investigate the effects of changing the chain length, grafting density, and the core volume fraction on the core pair probability at $T^* = 1$ and $\rho_b \approx 0.77$. In Fig. 5, we choose the case of $f = 25$, $N_m = 10$, $R_g/a_c = 0.540$, and $\phi_c = 0.169$ to be our base system and compare $g_{cc}(r)$ for different cases obtained from the theory and simulations. While in the simulations at fixed T^* and ρ_b we cannot vary the grafting density or the chain length without changing ϕ_c, in the theory we can change the geometrical parameters independently. In the following comparison, we retain the same LJ attraction among the monomers under $T^* = 1$ and atmospheric pressure. Therefore, when we change R_g or f but not ϕ_c in the theory we vary the number of beads in the cluster forming an oligomer. Figure 5(a) illustrates the theoretical predictions when we maintain a constant grafting density. If we first change the radius of gyration without changing the core volume fraction (curve (2)), we find that increasing the radius of gyration has a softening effect on the core pair probability yielding damped peaks compared with the

base case; the first peak is shifted outward slightly while the outward shift of the second peak is more pronounced. If we then decrease ϕ_c with increasing R_g, the softening effect progresses and the peaks are shifted further because the stretched oligomers at lower core volume fraction increase the range of the interparticle interactions. The simulation results in Fig. 5(c), curve (2) for the corresponding 15-mer system shows a similar lowering and outward shift of the peaks relative to the 10-mer system. Figure 5(b) shows the theoretical predictions of the pair probability changes when the radius of gyration is fixed. If we first double the grafting density without varying the core volume fraction (curve (2)), the increased oligomer grafting density yields a stronger oligomer mediated interaction and a more structured $g_{cc}(r)$. If we then decrease ϕ_c with increasing f (curve (3)), the peaks in $g_{cc}(r)$ are even more pronounced and the separation between the first and second peaks is reduced relative to the base case. Even though the core concentration is quite low ($\phi_c < 0.1$), high grafting density at small R_g/a_c yields a stronger entropic attraction among the particles. The simulation results in curve (3) of Fig. 5(c) qualitatively agree with the theoretical prediction of higher peaks and a smaller distance between the first and second peak of the pair probability. Both the first and second peaks in the simulation are shifted outward at higher grafting density relative to the base case. This effect is not captured by the theory. At such a high grafting density there could be non-negligible packing/layering effects of the monomer beads which yields even larger effective core size.

While the structural changes due to variations in the geometry of NOHMs at a fixed low temperature provide direct information about how the incompressible, space-filling oligomers influence the distribution of nanoparticles in the absence of solvent, temperature plays a more complex role in determining the equilibrium structure of the NOHMs system. When temperature changes, the importance of the LJ attraction relative to the thermal energy also changes. As these variations occur at fixed chain length and surface grafting density, the equilibrium core volume fraction and the monomer number density change to achieve the atmospheric pressure condition. As can be seen from Fig. 6, the core–core radial distribution function for systems with different chain lengths at various temperatures generally exhibits typical liquid-like behavior. In all cases the core particles are well dispersed with a single length scale of the core size shown in g_{cc}. This implies that the attached chains prevent the cores from aggregating. From the simulation results as well as the representative theoretical results, we see that as temperature increases the positions of the peaks are shifted outward. Under the zero pressure condition, increasing T^* results in decreased ϕ_c. In the theory, one can vary T^* and ϕ_c independently. When the system is more compressible at higher T^*, we expect to see less structured g_{cc} with more damped peaks for a given ϕ_c. However, lower core volume fraction leads to larger interparticle spacing for oligomers to fill, which then produces a stronger tendency for oligomers to stretch out and should yield more enhanced and shifted peaks in g_{cc}. The net effect of changing both T^* and ϕ_c is to shift the first peak of g_{cc} outward with little change in its height as seen in the theoretical results of Fig. 6(c) and the simulations in Fig. 6(b).

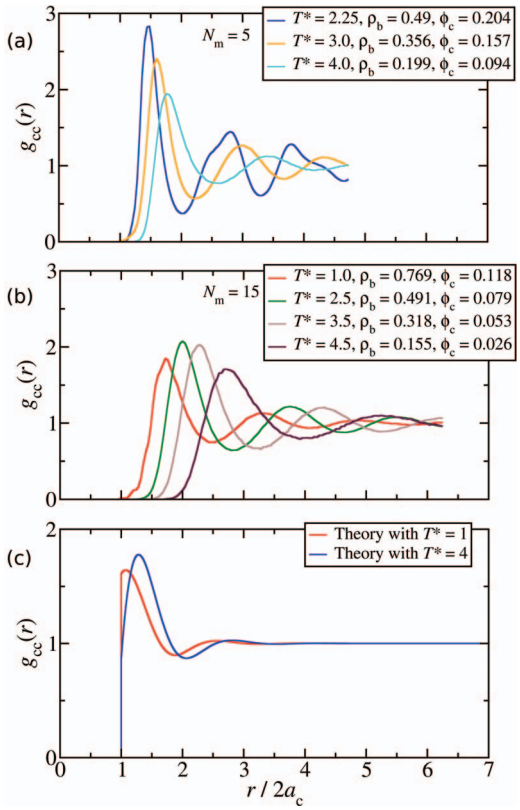

FIG. 6. Radial distribution function for nanoparticles at various temperatures: (a) simulation results for $N_m = 5$; (b) simulation results for $N_m = 15$; and (c) theoretical results for $R_g/a = 0.652$ corresponding to $N_m = 15$.

While the theory and simulation in Figs. 6(c) and 6(b) both predict an outward shift of the peak of the radial distribution function for $N_m = 15$, the shift is much more dramatic in the simulations. We believe that this difference arises from an enhancement of the steric repulsion between the NOHMs in the simulations with increasing T^* due to changes in the chain configuration. In the simulations, the increasing temperature at a given pressure leads to significantly smaller monomer number densities in the fluid phase. The small values of ρ_b at large T^* imply a significant amount of free space among the monomers which might be viewed as being filled with an added "phantom solvent" that reduces the "net" monomer–monomer attraction. As a result, increasing T^* is equivalent to creating a better solvent condition for the hairs and making the monomer–monomer excluded volume more important. This enhanced excluded volume will make the oligomer brushes expand providing steric repulsion between the cores at increasing radial distances. This excluded volume effect is not captured in the theory where we use an ideal freely jointed chain to set the radius of gyration of the linear-spring-bead oligomers.

The outward shift of the first peak in g_{cc} in the simulations in Fig. 6(b) due to better solvent conditions at increasing temperature is consistent with previous studies of star polymer solutions[27] and sterically stablized colloidal suspensions.[43] In Ref. 27 a pairwise additive steric repulsive potential was used to model the interactions of star polymers in solution. The range of this repulsion was set based

on experimental observations of the hydrodynamic radius of the polymers which was observed to increase with increasing temperature. The simulations then showed that the first peak in the radial distribution function shifted outward with increasing temperature. In a similar manner, Ref. 43 modelled sterically stabilized colloids using an interparticle potential with an effective hard-sphere diameter that included the brush height. The brush height increased with increasing Kuhn step and temperature.

The outward shift of the peak of the radial distribution function for NOHMs with shorter oligomers, $N_m = 5$, illustrated in Fig. 6(a) is smaller than for NOHMs with longer oligomers, $N_m = 15$, illustrated in Fig. 6(b). In the theory, the shorter oligomers yield a stronger entropic attraction because it is harder for the short, stiff oligomers to fill the interparticle space. The theory, therefore, also predicts a more modest outward shift in the peak for shorter oligomers. At the lowest temperature $T^* = 2.25$, the simulation results for $N_m = 5$ exhibit solid-like features such as a highly enhanced first peak and a split in the second peak. As the temperature is decreased further for this case, the dynamics of the system slow to the point where an equilibrium state was not computationally accessible.

As one measure of the oligomeric-fluid structure, we considered the pair correlation function for an oligomer bead relative to a core center $g_{cb}(r)$, which is plotted along with $g_{cc}(r)$ for $T^* = 4.5$ and 2.0 in Figs. 7(a) and 7(b). At $T^* = 2.0$, $g_{cb}(r)$ has three peaks near the core particle ($r < 5\sigma$) corresponding to the packing of the first layers of oligomer beads in the brush. At larger distances, $g_{cb}(r)$ decays and reaches a minimum, $r \approx 8.6\sigma$. As seen in Fig. 7, this minimum is correlated with the first peak observed in the $g_{cc}(r)$. This is understandable, since the probability of finding an oligomer bead at that distance is reduced due to the volume of the nearest neighboring cores. These correlations, although not as pronounced, extend to larger distances. As we increase the temperature (decrease density) these correlations become weaker and at $T^* = 4.5$ the minimum de-correlates and occurs at a position different than the position of the first peak of $g_{cc}(r)$. If the oligomeric fluid were incompressible, as it would be for small enough T^*, the oligomer bead density in the available fluid space, $\rho_b^t(r) = \rho_b g_{cb}(r)(1-\phi_c)/\phi_f(r)$, would be independent of radial position. In Fig. 7(b) we see that the bead density has a weaker variation than $g_{cb}(r)$ indicating that oligomers are attempting to fill the space between the cores but not doing so uniformly. At $T^* = 4.5$, the variations of the fluid density are as strong as the variations of $g_{cb}(r)$ suggesting that the oligomeric fluid is highly compressible.

Temperature also affects the extent of density fluctuations at different length scales, as characterized by the static structure factor at different wave numbers. From the theoretical predictions, we can see that the general behavior of the static structure factor for the system of $f = 25$, $N_m = 10$, and $R_g/a_c = 0.540$ shown in Fig. 8(a) at three different temperatures remains the same as that illustrated in Fig. 3. In particular, with decreasing q we see hard-core correlations followed by a plateau region with suppressed density fluctuations and finally the curve rises to the value of the reference hard sphere suspension at $q = 0$. As T^* increases the region of suppressed S corresponding to a deficit of neighboring particles occurs at smaller q and the value of $S(q)$ in the plateau region, $q \cdot 2a_c \sim 0.2 - 2$, is larger. These observations indicate that the system is more compressible at higher temperatures. The theoretical predictions agree qualitatively with the simulation results in terms of the location and depth of the particle deficit region. The simulations show enhanced peaks in the hard-core correlation region due to the steric repulsion associated with the chain packing, an effect that is absent in the theory because of the neglect of the effect of chain

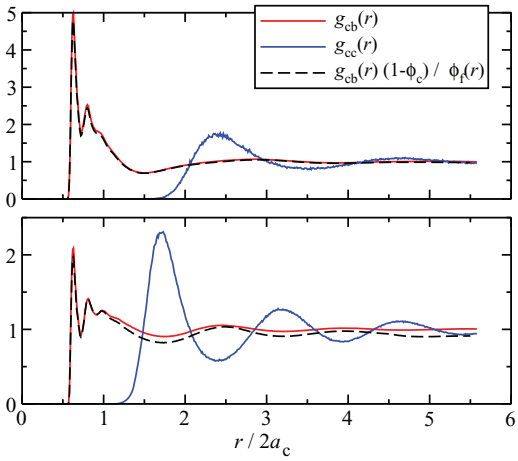

FIG. 7. Simulation results for core-core and core-bead correlation functions for two different temperatures for systems with nanoparticles with chain length $N_m = 10$. (top) $T^* = 4.5$; (bottom) $T^* = 2.0$.

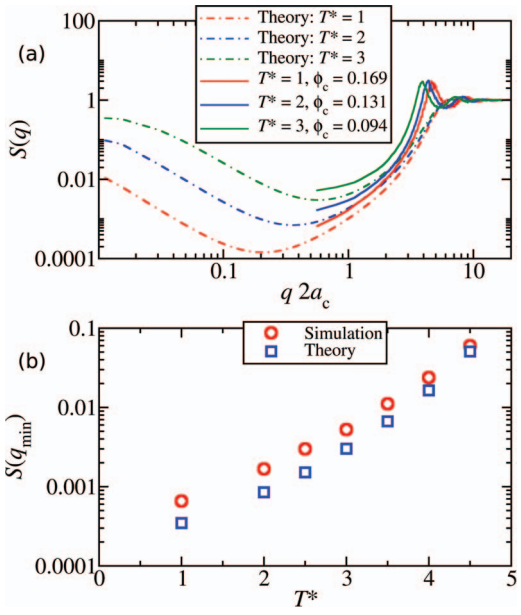

FIG. 8. (a) The static structure factor S as a function of the scaled wave number $q \cdot 2a_c$ for the system with $f = 25$ and $N_m = 10$ at different T^* predicted by the theory and the simulations. (b) The value of S at $q \cdot 2a_c \approx 0.56$, the smallest wave number accessible in the simulations for the same system, as a function of T^* predicted by the simulations and the theory. At each temperature ϕ_c and ρ_b for the theory are the same as the corresponding simulation values. Error bars for the simulation data in part (b) are smaller than the symbol size.

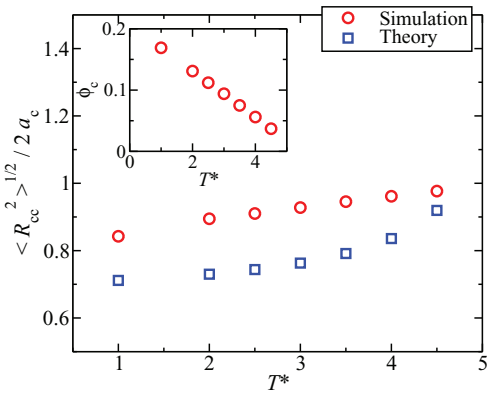

FIG. 9. Root-mean-square distance between the chain center of mass and the core center for the system of $f = 25$ and $N_m = 10$ as a function of T^* predicted by the simulations and the theory. At each temperature ϕ_c and ρ_b for the theory are the same as the corresponding simulation values. The inset shows simulation results of ϕ_c as a function of temperature. Error bars for the simulation data are smaller than the symbol size.

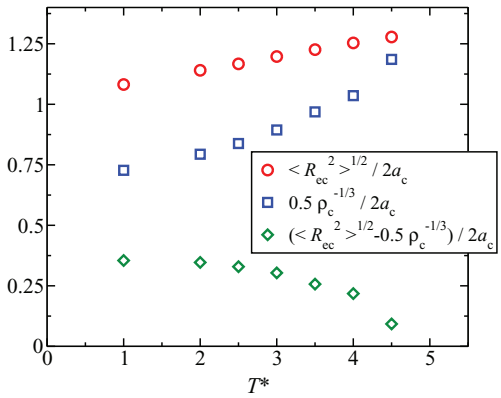

FIG. 10. Simulation results for the degree of interpenetration between the nanoparticles with $N_m = 10$ (diamonds), with the square-root of the mean-square of end-to-center distance (circles), and an estimate of the average distance between the core particles (squares). Error bars are smaller than the symbol size.

packing on their conformations. The value of $S(0)$ determines the compressibility of the single-component NOHMs fluid. In the simulations, we can estimate the compressibility from the $S(q)$ value at the smallest wave number q_{min} allowed by the periodic boundary conditions. As can be seen from Fig. 8(b), the compressibility of the system increases with temperature and the theoretical values of $S(q_{min})$ are reasonably close to the simulation results at all temperatures.

We turn now to characterizing the structure of the oligomer brushes attached to the cores. In our theory, the chain configuration is captured by a linear spring with all the monomers belonging to a chain being placed at the same position, the free end of the tethered spring. Therefore, the quantity that the theory can predict directly is the root-mean-square distance between the chain center of mass and the core center, $\langle R_{cc}^2 \rangle^{1/2}$. In Fig. 9, we compare theoretical and simulation results for this measure of the chain stretching for NOHMs with $f = 25$, $N_m = 10$, and $R_g/a_c = 0.54$ at different T^*. As shown in the inset of this figure, each temperature corresponds to a different core volume fraction from the simulations and higher T^* leads to lower ϕ_c. The theory indicates that chains must stretch to fill the interparticle space so that $\langle R_{cc}^2 \rangle^{1/2}$ grows with decreasing ϕ_c corresponding to increasing T^*. The simulation shows a similar trend although the chain stretches less at high T^* than predicted by the theory. The quantitative differences between the theory and simulation indicate limitations of the theory resulting from the assumption of ideal freely jointed chains. These differences are likely to increase when chain packing effects become more important, in particular for higher grafting densities than the ones studied in this work.

A measure of the chain conformation that provides more insight into the tendency of oligomer brushes on neighboring particles to interpenetrate is the root-mean-square distance between the center of the core and the ends of its tethered oligomer chains, $\langle R_{ce}^2 \rangle^{1/2}$. The average core–core separation can be approximated using the core number density as $\rho_c^{-1/3}$. We can then define the degree of interpenetration as the difference between $\langle R_{ce}^2 \rangle^{1/2}$ and $\rho_c^{-1/3}/2$. From the representative simulation results shown in Fig. 10 for $N_m = 10$, we find that the mean-square end-to-center distance increases with temperature consistent with the results for $\langle R_{cc}^2 \rangle^{1/2}$ in Fig. 9. As noted above, a part of this increase is caused by the tendency of the chains to fill the interparticle space and is consistent with the increase in $\rho_c^{-1/3}$. However, if we examine the interpenetration, we observe two temperature regimes. Below a threshold of $T^* \approx 2.5$, the interpenetration is constant suggesting that the chains cooperate to fill the interparticle space as predicted by the theory. At higher temperatures, however, the interpenetration decreases with increasing temperature. At these high temperatures, the monomer–monomer attraction is small and the chains are filled with void space which may be viewed as a phantom solvent. The NOHMs then begin to act like star polymers[44] or sterically stabilized colloids[43] in a theta or good solvent where the strong excluded volume of the star arms/brushes leads to entropic repulsion between the stars/colloids. The brush then expands with increasing temperature as the solvent quality becomes better[45] and the strong steric repulsion of the brushes decreases the interpenetration of the brushes of neighboring NOHMs.

Finally, it is of interest to see how much freedom the core has to wander relative to its tethered oligomers. This is quantified by the average distance between the center of the core, $\mathbf{r}_c$, and the center-of-mass of the corona, $\mathbf{r}_{cm}$. Figure 11 shows this distance normalized by the root-mean-square end to center distance $\langle R_{ce}^2 \rangle^{1/2}$ as function of temperature. The results show that the core of NOHMs with large chains can deviate significantly from the corona center-of-mass particularly at lower temperatures. Under these conditions the chains strongly interpenetrate and the interstitial space is filled by a fluid of oligomers tethered to many neighboring cores as envisioned by the theory. The chains and core then can sample many possible configurations while the chains still fill the interstitial space. Smaller chains give less possible configurations and the core is closer to the center of its tethered oligomers. At high temperatures, the chains stretch because they are in a phantom solvent and again this reduces

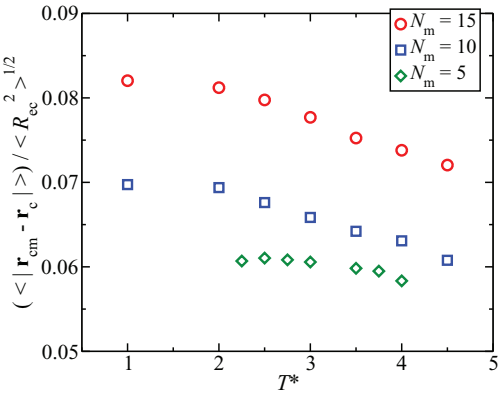

FIG. 11. Simulation results for the average distance of the core from the center of mass of the oligomer corona for different chain lengths as function of temperature. Error bars are smaller than the symbol size.

the freedom of the core to move relative to the center of mass of its tethered oligomers.

V. CONCLUSIONS

We have used coarse-grained molecular dynamics simulations and density-functional theory to explore the equilibrium structure of NOHMs, which consist of nanoparticles with grafted oligomeric chains and no added explicit solvent. The simulations and theory confirm the experimental observation that the geometry of NOHMs including nanoparticle size and oligomer molecular weight can strongly influence the properties of these fluids.

At low temperatures and for oligomers with 10 or 15 monomer beads, the qualitative trends in the simulated NOHMs structure can be explained by a density-functional theory that treats the tethered oligomers as a fluid that fills the interparticle space. This tethered fluid experiences an entropic penalty when the chains must stretch to fill the interstices and an enthalpic penalty when the local fluid density changes. In particular both theory and simulations show that the structure factor at small wave numbers is greatly reduced relative to the reference hard sphere value. The reduction in the structure factor increases with decreasing temperature as the oligomeric fluid becomes less compressible. The requirement that the oligomers fill the interstitial space leads to an entropic attraction between the cores, which causes the peak of the core–core pair distribution function to be larger than that of a hard sphere suspension with the effect increasing with decreasing chain length. At moderate temperatures, the chains stretch in proportion to the increase in the interparticle spacing as predicted by the theory.

At higher temperatures, the chains expand faster than the interparticle spacing and the increase in the brush height is larger than that predicted by the theory. The radial position of the first peak of the core–core pair distribution also increases at high temperature at a rate larger than that predicted by the theory. At temperatures larger than $T^* \approx 2.5$ the density of oligomer beads within the interstitial fluid decreases and the void spaces between the monomers may be viewed as being filled by a phantom solvent. The trends seen in the simulations are then consistent with previous results for star polymers and polymer-stabilized colloids in solvents. In particular, the increased brush height can be attributed to the increasingly good solvent quality at higher temperatures. Likewise, the outward shift of the peak in the pair distribution function can be attributed to an increasingly strong steric repulsion associated with oligomer brushes in good or theta solvents.

ACKNOWLEDGMENTS

The authors would like to thank Professor Fernando Escobedo for suggesting the simulation model used in this work and for helpful discussions. This publication is based on work supported in part by Award No. KUS-C1-018-02, made by King Abdullah University of Science and Technology (KAUST). Additional support was provided by Grant No. DE-SC-0002128 from the (U.S.) Department of Energy (DOE), Office of Basic Energy Sciences and Grant No. CBET-1033155 from National Science Foundation (NSF).

[1] J.-P. Hansen and I. R. McDonald, *Theory of simple liquids* (Academic, Cambridge, 2006).
[2] P. N. Pusey, *Colloidal Suspensions in Liquids Freezing and Glass Transition* (Elsevier, Amsterdam, 1991).
[3] M. E. Cates and M. R. Evans, *Soft and Fragile Matter: Non-equilibrium Dynamics, Metastability and Flow* (Institute of Physics, Bristol, 2000).
[4] G. D. Smith, D. Bedrov, L. Li, and O. Byutner, J. Chem. Phys. **117**, 9478 (2002).
[5] L. S. Schandler, L. C. Brinson, and W. G. Sawyer, JOM **59**, 53 (2007).
[6] J. A. Eastman, S. U.S. Choi, S. Li, W. Lu, and L. J. Thompson, Appl. Phys. Lett. **78**, 718 (2001).
[7] R. Prasher, Phys. Rev. Lett. **94**, 025901 (2005).
[8] M. Anyfantakis, A. Bourlinos, D. Vlassopoulos, G. Fytas, E. Giannelis, and S. K. Kumar, Soft Matter **5**, 4256 (2009).
[9] P. Voundouris, J. Choi, H. Dong, M. R. Bockstaller, K. Matyjaszewski, and G. Fytas, Macromolecules **42**, 2721 (2009).
[10] P. Akcora, H. Liu, S. K. Kumar, J. Moll, Y. Li, B. C. Benicewicz, L. S. Schadler, D. Acehan, A. Z. Panagiotopoulos, V. Pryamitsyn, V. Ganesan, J. Ilavsky, P. Thiyagarajan, R. H. Colby, and J. F. Douglas, Nature Mater. **8**, 354 (2009).
[11] Z. Zhang, M. A. Horsch, M. H. Lamm, and S. C. Glotzer, Nano Lett. **3**, 1341 (2003).
[12] D. Nykypanchuk, M. M. Maye, D. van der Lelie, and O. Gang, Nature (London) **451**, 549 (2008).
[13] J. L. Nugent, S. S. Moganty, and L. A. Archer, Adv. Mater. **22**, 3677 (2010).
[14] A. B. Bourlinos, R. Herrera, N. Chalkias, D. D. Jiang, L. A. Archer, and E. P. Giannelis, Adv. Mater. **17**, 234 (2005).
[15] A. B. Bourlinos, S. R. Chowdhury, R. Herrera, N. Chalkias, D. D. Jiang, L. A. Archer, and E. P. Giannelis, Adv. Funct. Mater. **15**, 1285 (2005).
[16] A. B. Bourlinos, E. P. Giannelis, Q. Zhang, L. A. Archer, G. Floudas, and G. Fytas, J. Eur. Phys. E **20**, 109 (2006).
[17] R. Rodriguez, R. Herrera, L. A. Archer, and E. P. Giannelis, Adv. Mater. **20**, 4353 (2008).
[18] P. Agarwal, H. Qi, and L. A. Archer, Nano Lett. **10**, 111 (2010).
[19] F. L. Verso, S. A. E. A. Milchev, and K. Binder, J. Chem. Phys. **133**, 184901 (2010).
[20] M. Daoud and J. P. Cotton, J. Phys. **43**, 531 (1982).
[21] A. Halperin, M. Tirrell, and T. P. Lodge, Adv. Polym. Sci. **100**, 31 (1992).
[22] T. M. Birshtein and E. B. Zhulina, Polymer **30**, 170 (1989).
[23] S. Föster, E. Wenz, and P. Lindner, Phys. Rev. Lett. **77**, 95 (1996).
[24] L. Willner, O. Jucknischke, D. Richter, J. Roovers, L.-L. Zhou, P. M. Toporowshi, L. J. Fetters, J. S. Huang, M. Y. Lin, and N. Hadjichristidis, Macromolecules **27**, 3821 (1994).
[25] A. Halperin and J. F. Joanny, J. Phys. II **1**, 623 (1991).
[26] M. Kapnistos, D. Vlassopoulos, G. Fytas, K. Mortensen, G. Fleischer, and J. Roovers, Phys. Lett. **85**, 4072 (2000).
[27] A. N. Rissanou, D. Vlassopoulos, and I. A. Bitsanis, Phys. Rev. E **71**, 011402 (2005).
[28] A. Jayaraman and K. S. Schweizer, J. Chem. Phys. **128**, 164904 (2008).

[29]A. Jayaraman and K. S. Schweizer, Langmuir **24**, 11119 (2008).
[30]X. Zhang, Z. L. Zhang, and S. C. Glotzer, Nanotechnology **18**, 115706 (2007).
[31]M. A. Horsch, Z. Zhang, and S. C. Glotzer, Nano Lett. **6**, 2406 (2006).
[32]M. R. Wilson, A. B. Thomas, M. Dennison, and A. J. Masters, Soft Matter **5**, 363 (2009).
[33]E. R. Chan, L. C. Ho, and S. C. Glotzer, J. Chem. Phys. **125**, 064905 (2006).
[34]C. R. Iacovella, A. S. Keys, M. A. Horsch, and S. C. Glotzer, Phys. Rev. E **75**, 040801 (2007).
[35]H.-Y. Yu and D. Koch, Langmuir **26**, 16801 (2010).
[36]J. D. Weeks, D. Chandler, and H. C. Andersen, J. Chem. Phys. **54**, 5237 (1971).
[37]J. S. Smith, D. Bedrov, and G. D. Smith, Compos. Sci. Technol. **63**, 1599 (2003).
[38]S. J. Plimpton, J. Comput. Phys. **117**, 1 (1995).
[39]P. J. in't Veld, S. J. Plimpton, and G. S. Grest, Comput. Phys. Commun. **179**, 320 (2008).
[40]W. L. Mattice, C. V. Helfer, and A. P. Sokolov, Macromolecules **36**, 9924 (2003).
[41]F. F. Betancourt-Cárdenas, L. A. Galicia-Luna, and S. I. Sandler, Fluid Phase Equilib. **264**, 174 (2008).
[42]D. A. McQuarrie, *Statistical Mechanics* (University Science Books, Sausalito, 2000).
[43]U. Genz, B. D'Aguanno, J. Mewis, and R. Klein, Langmuir **10**, 2206 (1994).
[44]C. N. Likos, H. Löwen, M. Watzlawek, B. Abbas, O. Jucknischke, J. Allgaier, and D. Richter, Phys. Rev. Lett. **80**, 4450 (1998).
[45]M. Rubinstein and R. H. Colby, *Polymer Physics* (Oxford University Press, Oxford, 2003).